Title
Towards a Single Chemical Model for Understanding Lanthanide Hexaborides.

Journal
Angewandte Chemie (International ed. in English), 59(50)

ISSN
1433-7851

Authors
Munarriz, Julen
Robinson, Paul J
Alexandrova, Anastassia N

Publication Date
2020-12-01

DOI
10.1002/anie.202010638

Peer reviewed

COMMUNICATION

Towards a Single Chemical Model to Understand Lanthanide Hexaborides

Julen Munarriz,[a] Paul J. Robinson, [b] and Anastassia N. Alexandrova*[a,c]

[a] Dr. J. Munarriz, Prof. A. N. Alexandrova
Department of Chemistry and Biochemistry
University of California Los Angeles
Los Angeles, CA, 90095, USA
E-mail: ana@chem.ucla.edu
[b] P. J. Robinson
Department of Chemistry
Columbia University
New York, NY, 10027, USA
[c] Prof. A. N. Alexandrova
California NanoSystems Institute
University of California Los Angeles
Los Angeles, CA, 90095, USA

Supporting information for this article is given via a link at the end of the document.

Abstract: Lanthanide hexaborides (LnB_6) have disparate and often anomalous properties, from structurally homogeneous mixed valency, to superconductivity, spectral anomalies, and unexplained phase transitions. It is unclear how such a diversity of properties may arise in the solids of identical crystal structures and seemingly very similar electronic structures. Building on our previous model for SmB_6 (mixed valent, with a peak in specific heat, and pressure induced magnetic phase transitions), we present a unifying dynamic bonding model for LnB_6 that explains simultaneously EuB_6 (possessing an anomalous peak in specific heat at low T, magnetic phase transitions, and no mixed valency), YbB_6 (mixed valent topological insulator), and rather ordinary LaB_6. We show that Ln can engage in covalent bonding with boron, and, in some members of the LnB_6 family, also easily access alternative bonding states through the electron-phonon coupling. The accessibility, relative energetics, and bonding nature of the states involved dictate the properties.

Quantum Materials – materials that exhibit strong electron-phonon coupling – have many exotic and usually unexpected properties,[1,2] such as valence fluctuations,[3] quantum critical points,[4] (topological) Kondo insulating properties,[5] and heavy fermion superconductivity.[6]

Lanthanide hexaborides (LnB_6) are quantum materials that show a number of anomalous and seemingly contradictory features, in spite of having the same crystal structure (CaB_6-type, $Pm\bar{3}m$ space group, see Figure 1A).[7-12] For example, both EuB_6 and SmB_6 have an anomalous behavior in the specific heat as a function of temperature, *T* (the so-called Schottky anomaly).[13,14] Many electronic properties of SmB_6 and EuB_6, such as resistivity and electronic transport, are highly sensitive to *T* and pressure, *p*.[15,16] However, some other properties of these two alloys are very different: SmB_6 is Sm(II)/Sm(III) mixed-valent, whereas EuB_6 is not.[15] EuB_6 undergoes a second order ferromagnetic (FM) to paramagnetic (PM) phase transition at 15.6 K, which is absent in non-magnetic SmB_6. However, SmB_6 can become magnetic via phase transition at high *p*. Another unusual LnB_6 is YbB_6, proposed to be a moderately correlated topological insulator, similar to SmB_6, but with a larger bulk band gap.[7] There is a disagreement whether YbB_6 is single-valent, Yb(II),[17] or mixed-valent, Yb(II)/Yb(III).[7,18]

Despite much theoretical research,[19-21] many features of LnB_6 remain a mystery, and there is no unifying molecular-level framework that would simultaneously explain all their more and less exotic behaviors, and predict new ones. Here, we expect to advance in such unifying model of LnB_6, and pave the way towards the rational discovery of new quantum phases with selected properties. We build the model on the basis of LaB_6, EuB_6, YbB_6, (and SmB_6), as they cover a wide range of very different behaviors.

The electronic structure of LnB_6 is expected to be strongly correlated, requiring the high-level *ab initio* description,[22] which is inaccessible for periodic systems. Hence, we build the understanding of the material from the ground up, using minimal energy models informed by electronic structure.[23,24] In a previous study, we developed a dynamic bonding model for SmB_6 based on the non-trivial SmB_2^+ fragment,[25] which we selected by analyzing the electronic density distribution in the full solid, and

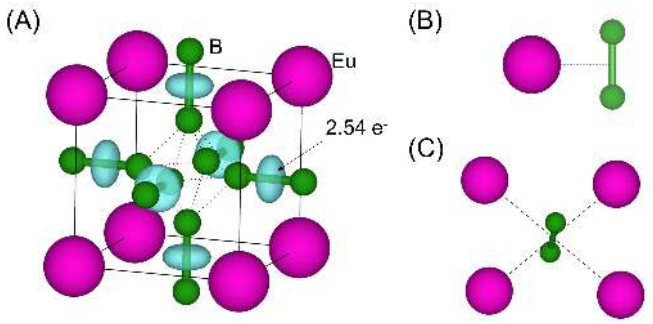

Figure 1. (A) Crystal structure of EuB_6 (and LnB_6 in general) and ELF basins (depicted in blue, isovalue = 0.75). The electron density integration over the di-synaptic B–B basins yields a population of 2.54 e^-. Notice that, for the sake of clarity, we have added the six B atoms bonded to the B atoms that are inside the unit cell. (B) Minimal cluster model: LnB_2^+. (C) Crystallographic face with a B_2 unit surrounded by 4 Ln atoms.

treated with high level multi-reference *ab initio* methods. The model revealed the existence of a low-barrier double-well potential with two different Sm–B_2 bonding modes. In the full solid, every B_2 accesses 4 Sm atoms in the face of a cubic cell (Figure 1C), producing 4 minima where one Sm is Sm(II) and bound to B_2 covalently, and 1 minimum where B_2 is in the center of the cubic face and Sm is Sm(III). The relative depths of the minima in the solid is predicted to be ~4.0 meV. The model yields B_2 acting as a shuttle of e^-, mediating the Sm(II)/Sm(III) mixed valence *via* vibronic coupling. It also provides a chemical explanation for the dependence of mixed valency on *T* and *p*.[16] The vibronic coupling between the two nearly-degenerate states reveals the additional energy of motion leading to the Schottky anomaly, as well as forbidden low-energy peaks in Raman spectra that appear only at low *T*. Namely, Raman spectroscopy (local-structure sensitive) showed that distortions of B_2 dimers are strongly electron-phonon coupled, thus supporting our local approach to the structure.

Any chemical bonding model should behave logically upon adding or removing electrons. Hence, the SmB_6-like model, if it is correct, should be flexible to explain the properties of other LnB_6.

The initial assessment of EuB_6 was done using the Electron Localization Function (ELF) with periodic-boundary-condition DFT (see SI for details). ELF provides a measure of the probability of finding electron pairs, e.g. covalent bonds and lone pairs.[26] The only thus-found covalent bonds in EuB_6 are in the B_2 units (Figure 1A).[19] Integration of the electron density over the ELF basins yielded a B–B bond population of 2.54 e^-, indicative of covalent bonds with a bond order of ~1.25. From the analysis of the electron density, the bond critical points only appear within the B_2 dimers, and between the center of B_2 and Eu atoms (Figure S3). This result is consistent with the DFT-optimized B–B distance within B_2 dimers (1.652 Å) being shorter than in the central octahedron (1.746 Å). Overall, the results point towards the main interactions in the material being within B_2, and Eu–B_2. Thus, we can expect the EuB_2^+ fragment to contain the main chemical interactions that are important in the solid. Notice that the positive charge is introduced to account for the under-coordinated environment of the minimal fragment with respect to the periodic material.[25] It is important to note that the three-atom model was validated by experiments for SmB_6. In this work, we aim to analyze whether the same framework, developed on the basis of the LnB_2^+ system, can be used to explain the behavior of other properties in the LnB_6 series.

The Potential Energy Surface (PES) EuB_2^+ was computed with 8-SA-CASSCF(14,10)/MRCI + DKH6, including the quintet and septet A_1, A_2, B_1 and B_2 states (Figure 2A,B). The active space orbitals are depicted in Figure 2C. The choice of the method was informed by our previous studies of Sm and Re borides (see the SI for details).[23,27] At this point, we highlight that, as previously introduced, the electronic structure of LnB_6 is very complicated, requiring the use of high level methods for attaining an accurate description.[22] Notice that there is a significant number of bonding Eu–B_2 molecular orbitals (MOs): $4a_1$, $1b_1$, $1b_2$, $3b_2$, and to a lesser extent $3a_1$, in line with recent reports on *d-p* Ln-B hybrid orbitals.[28] This fact points against the long assumed purely ionic character of Eu, and the bonding "innocence" of boron.

A double-well potential with an energy difference, ε, between the two minima of only 2.2 meV was found for EuB_2^+ (Figure 2A). ε computed for the small model is an estimate of the value for the solid. The *"short"* minimum (highlighted in red in Figure 2C) has the Eu–B_2 distance of 2.13 Å, and the B–B distance of 1.60 Å, and is predominantly $^7A_1$. The *"long"* minimum (highlighted in blue in Figure 2C) has the Eu–B_2 distance of 2.23 Å, and the B–B distance of 1.55 Å, and is predominantly $^5A_1$. The small difference in the Eu–B_2 distance, in conjunction with the near-degeneracy of the two minima, indicates that the interconversion between the states can be achievable through vibrations. Hence, EuB_6 could exhibit subtle geometrical distortions (by accessing the *"short"* minima), which have been proposed by Martinho et al.,[29] who also related the distortions to the appearance of two symmetry-forbidden peaks in the Raman spectrum.

The electronic configurations of the two minima are nearly identical, and only differ by one electron shifting from $1a_1$ to $3a_1$, as the system goes from the "*long*" to the "*short*" minimum (Figure 2C). $1a_1$ is the isolated π_{2px} MO of the B_2 fragment, and the $3a_1$ is mainly the σ_{2pz} MO of B_2. Note that the short B–B distance normally makes the π_{2px} MO more stable than σ_{2pz}. Nonetheless,

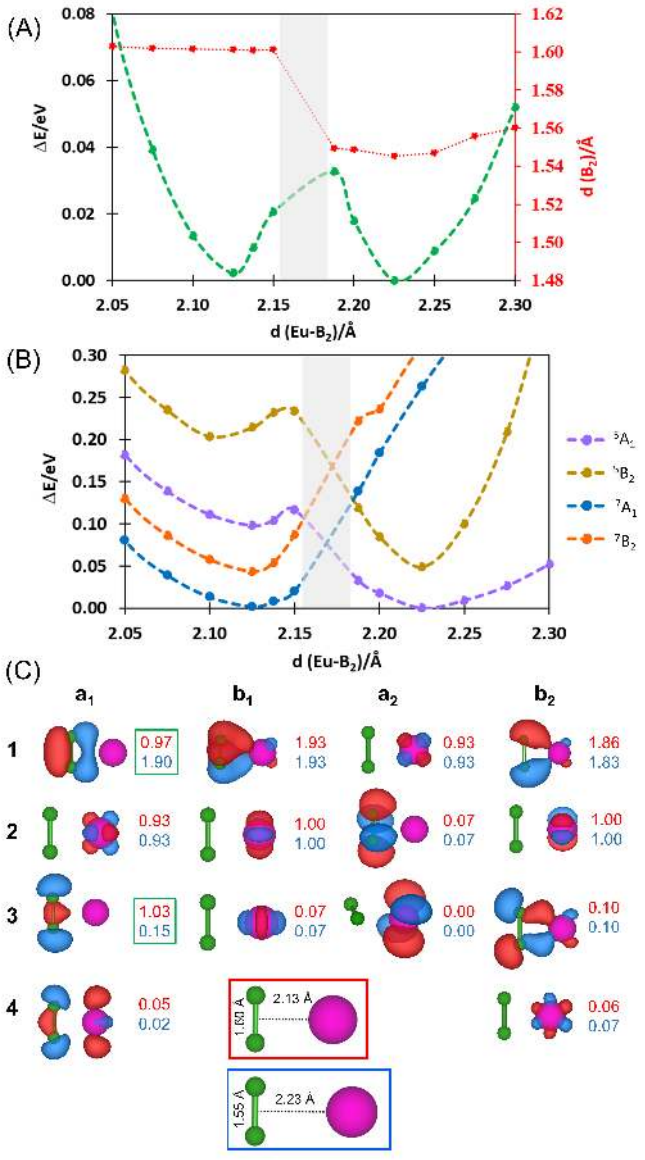

Figure 2. EuB_2^+ minimal cluster model. (A) Ground state energy (green) and corresponding B_2 bond length (red). (B) Potential Energy Surface corresponding to the four lowest-lying states. No convergence was achieved in the area depicted in gray. (C) The CAS active space orbitals, and the occupations for the two minima. The geometries of the two minima are shown in the insets: the "*short*" minimum with the shorter Eu–B_2 distance is outlined in red, and the "*long*" minimum is outlined in blue.

the proximity of the Eu cation, and the increased B–B distance in the "*short*" minimum compared to the isolated dimer stabilize σ_{2pz}. Interestingly, the experimental observations show that Eu (II) in EuB_6 is the stable state, which remains unaltered even under external *p* of up to 25 GPa.[15] This is contrary to what happens in SmB_6 where *p* induces a phase transition from a mixed valent to the pure Sm(III) state.[25] Thus, we propose that in the solid EuB_6, the two Eu–B_2 bonding states also co-exist, and the vibronic coupling between the two states is achieved via nuclear motion (Figure 1C), analogously to SmB_6, but without driving mixed valency.

Both SmB_6 and EuB_6 exhibit an anomalous peak in the specific heat (C_V) at low *T*. Notice that C_V is the derivative of the energy with respect to *T* at constant volume, and thus, one would expect that the internal energy increases with *T*, as it happens in LaB_6 (Figure 3A).[13] The presence of an anomalous peak points towards the existence of an additional energy scale of motion.[30] On the basis of the two-minima model and statistical thermodynamics, we previously proposed an analytic expression for C_V in the low-*T* regime, which can be applied to EuB_6:[25]

$$C_V = \frac{1}{T^2}\cdot\frac{d\cdot\varepsilon^2\exp(\varepsilon\cdot\beta)}{(1+d\cdot\exp(\varepsilon\cdot\beta))^2} \qquad (1)$$

where k_b is the Boltzmann constant, β is $(k_b\cdot T)^{-1}$, and *d* is the system degeneracy. In this family of materials, $d = 4$, as each B_2 unit is surrounded by 4 Ln atoms.

Using $\varepsilon = 2.2$ meV for the energy splitting in EuB_6, a peak in the specific heat is predicted to occur at T_P ~12 K. This result is in very good agreement with the reported experimental value of ~10.5 K (Figure 3B),[31,32] especially considering the minimalism of the model used to derive ε. Because ε in SmB_6 is larger than in EuB_6 (4.0 vs 2.2 meV), the anomaly in EuB_6 occurs at a lower *T* (12 K vs 20 K),[13] in agreement with the experiment. Notice that for EuB_6 a second peak in C_V appears at the Curie Temperature (T_C)

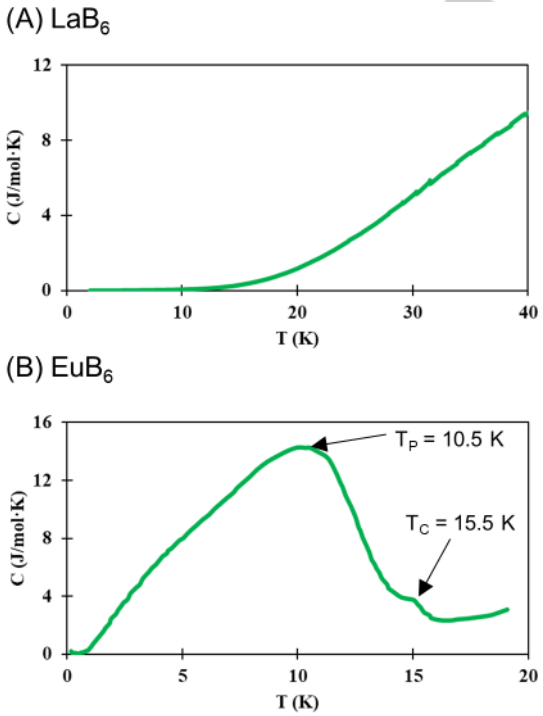

Figure3. Representation of the heat capacity against the temperature of (A) LaB_6 and (B) EuB_6. The data has been extracted from references 13 and 14, respectively.

of 15.5 K,[14] which has been reported to be a consequence of the system transition from FM to PM at T_C.[32] At this point, we also note that the presence of low lying excited states (like $^7B_2$ and $^5B_2$) may also be relevant for explaining such phenomena, as a consequence of low energy (less than 0.1 eV) electronic transitions.

Next, we consider two additional extremes in the LnB_6 series: YbB_6 and LaB_6, which differ in properties quite dramatically. YbB_6 has been proposed to be both Yb(II/III) mixed valent, and Yb(II) single valent.[7,17,18] The ELF in the YbB_6 solid shows the same pattern as for EuB_6 and SmB_6 (Figure S4A). The electron population in the B–B bond is 2.58 e^-, very similar to that in EuB_6 (2.54 e^-). This points towards the adequacy of the YbB_2^+ fragment in the minimalistic description of the material. Its PES was studied using 4-SA-CASSCF(11,13)/MRCI + DKH6, i.e. with the same active space as for EuB_2^+, but removing the unoccupied $3a_2$ MO and other 3 *f*-AOs that stay doubly occupied and inactive. Moreover, we needed the 4-SA to keep the 4 *f* orbitals in the active space (see Computational Details in the SI for further details). The PES shape for YbB_2^+ is very different from that of EuB_2^+ (Figure 4A): there is only one ground state minimum ($^2B_1$), and 4 low-lying doublet states whose PESs are nearly parallel to the ground state. These excited states correspond to electronic transitions between the single-unoccupied *f* orbital.

This picture signals the existence of a single bonding mode within YbB_6, with Yb not switching valency through phonons and remaining either single valent, or divalent but such that some Yb atoms are Yb(II) and others are Yb(III), as suggested by some authors.[7,18] To the best of our knowledge, no Schottky anomalies have been reported for YbB_6, in agreement with the model.[33,34] However, it has been noted that the heat capacity increases more rapidly than expected at 15 K,[34] and that at $p > 18$ GPa a transition to a mixed-valent state occurs with an anomaly in the T_{2g} mode for the B.[35] We hypothesize that these could be driven by the presence of the very close-in-energy electronic states, $^2A_1$ and $^2B_1$, in the YbB_2^+, which are only 25 meV apart, and differ by the populations of non-bonding *f*-orbitals. The transition between them at low *T* might create an additional electronic energy scale affecting the heat capacity. Consistent with the model, YbB_6 (as CaB_6) do not have anomalies in the Raman spectra,[29,36] whereas EuB_6, SmB_6, and CeB_6 have both more pronounced anomalies in the heat capacity, and Raman anomalies at about 200 cm^{-1}.

Next, we address LaB_6, whose ELF (Figure S4B) reveals an electron population of 2.62 e^- for the B–B basin, very similar to those in EuB_6 and YbB_6 in spite of the change in the atomic number. The cluster model, LaB_2^+, was computed at the 2-SA-CASSCF(11,8)/MRCI + DKH4 level of theory (see the SI for details). The PES shape is significantly different from those of EuB_2^+ and YbB_2^+. The ground state consists of the $^1A_1$ and $^3A_1$ terms, which cross at R(La-B_2)=2.24 Å producing a "shoulder" (Figure 4B). The energy splitting between the two states is 104 meV, significantly greater than in EuB_2^+, making the $^3A_1$ minimum less accessible. Notice that the electronic transition between the two states is the same as in EuB_2^+ (Figures 2 and S2). The Ln–B_2 distance between the two minima is also 70 % greater: 0.17 Å, vs 0.10 Å in EuB_2^+. In addition, the $^3A_1$ minimum might not support a ZPE. Given that for all hexaborides studied so far, the cluster models gave nearly quantitative information about the full solid, we may conclude that in LaB_6 the $^3A_1$ minimum is not populated through phonon motion. This agrees with the lack of the Schottky anomaly at low *T*.[33] Nonetheless, the model reveals the effective

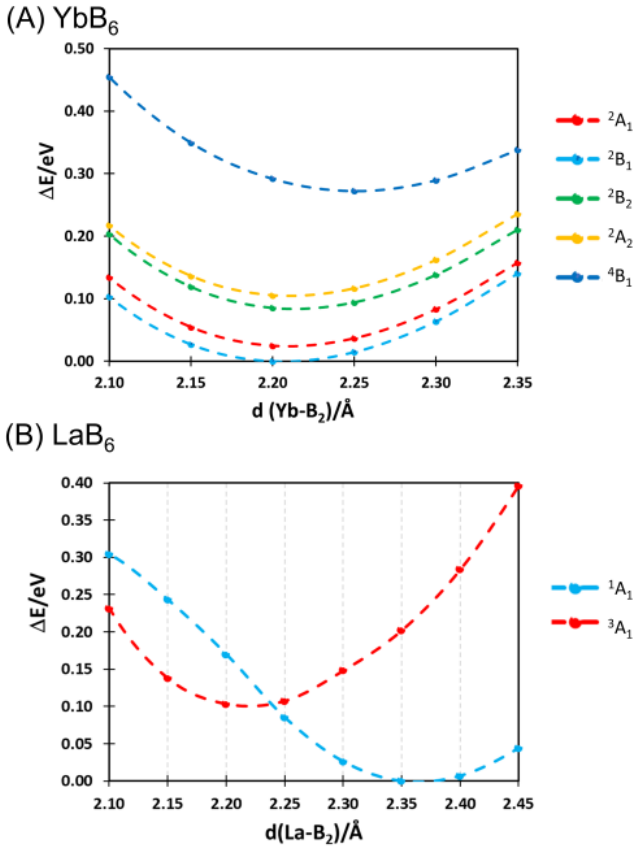

Figure 4. Potential Energy Surface for: (A) YbB_2^+ minimal cluster model; and (B) LaB_2^+ minimal cluster model.

widening of the potential at higher energies toward inclusion of the second minimum, which may explain the appearance of an unusual bump in the heat capacity at ~50 K.[37] Moreover, contrarily to EuB_2^+ and YbB_2^+, LaB_2^+ has no other low-lying excited states (as a consequence of the absence of occupied *f*-orbitals and transitions between them), which is likely to explain the absence of low-*T* effects.

So far, it appears that the chemical model proposed here is descriptive of many features along the LnB_6 series, relating electronic structure to diverse properties. The difference in which the minima are accessed by the motion of boron arises from the difference in the *f*-electron configuration in Ln.

Further, known and hypothesized binary $Ln_xLn'_{1-x}B_6$ alloys can be examined within our model. The LnB_6 series has only a 0.06 Å range in lattice constants,[38] and a number of such solid solutions have been characterized.[39,40] For example, the average valence of SmB_6 increases upon doping with Yb, and decreases upon doping with La.[41] In our model, these effects can be linked to changing the relative depths (hence, populations) of the two Sm-B_2 minima due to the presence of another Ln in the cubic face.

Magnetic susceptibility and conductivity of $Eu_{1-x}La_xB_6$ have been known for quite some time.[42] The solid transitions from a semiconductor to metallic beneath x=0.01.[43] Additionally, a number of studies have explored the anomalous magnetic transport and magnetic phase transitions as a function of doping.[44-46] A Raman study of magnetic phases for $x \leq 0.05$ found a magnetic polaron state, which could not be confirmed to have any phonon contribution, and perhaps ruling out any large scale displacements demanded by Jahn-Teller polarons.[43] A later Raman study of several $x \leq 0.2$ reported a local symmetry breaking of the boron units.[47] Our model suggests that Eu_{1-x}(La or $Yb)_xB_6$ transitions from a mixed-minima state to a mostly single minima state with increasing x, consistent with with the valence transition seen in Sm_{1-x}(La or $Yb)_xB_6$. The emergent strong anharmonicity may have a large effect on transport properties.

For $La_{1-x}(Eu_x)B_6$, Eu-B_2 is expected to thermally access different electronic states. However, the relative depths of the wells are likely to change as a function of x, affecting the *T* at which they can be populated. The valence-*T* dependence should show a smooth transition as a function of x. We expect a similar situation in $Eu_{1-x}Yb_xB_6$. Yb has a filled rather than empty f-shell, and also no a permanent magnetic moment. The $Eu(Sm)_xLa(Yb)_{1-x}B_6$ example suggests a mechanism to turn mixed valency on or off consistent with available experiment.[39]

Alloying is generally likely to create more states of Ln with the boron, and vary their energy splitting. This would result in a more complicated behavior of the specific heat, e.g. appearance/disappearance of shifts of the Schottky anomaly in the direction dependent on the signs of the exchange interactions. This overall more complicated energy landscape of the alloys may produce new types of vibronic resonances, opening interesting technological opportunities.

Finally, we suggest how the proposed vibronic effects in LnB_6 could be experimentally detected. A useful probe would be the T1 relaxation rate as a function of *T* in NMR. For example, in clathrates, "rattling phonons" give rise to a characteristic T1-*T* relationship deviating from the harmonic phonons response,[48] but well-modeled by a double-well potential.[49] Indeed, SmB_6 was shown to have an applied-field-dependent anomalous relaxation rate, consistent with theories of in-gap states.[50] We expect that by turning on or off the availability of multiple bonding minima through alloying, the anomaly in the T1 relaxation rate would commensurately appear/disappear with the mixed valency. Angle resolved photoelectron spectroscopy (ARPES) can directly measure the band structure, and was able to detect the topological difference between the bands of LaB_6 and SmB_6 as well as other borides, which arise from differences in Ln valence.[51] The symmetry-forbidden low-energy Raman features may shift in energy and intensity, or disappear upon alloying a two-states LnB_6 with another Ln. The Fano shape of the A_{1g} peak seen in pure SmB_6[25] may report on the concentration of a co-alloying Ln.

Overall, we expect to have advanced on the understanding of LnB_6 systems. The bonding indicators are in agreement with the three-atom cluster model proposed, and the cluster PES is consistent with the experimental properties under study. Thus, we believe the proposed model can be useful to the scientific community. We highlight the relevance of the model on predicting and explaining many system properties at an atomic level and propose experimental procedures to validate our conclusions.

Acknowledgements

We thank the Institute for Digital Research and Education at UCLA and the Extreme Science and Engineering Discovery Environment for supercomputer time. A.N.A. acknowledges the support of the NSF CAREER Award (CHE-1351968). P.J.R. acknowledges support from the National Science Foundation Graduate Research Fellowship (DGE-1644869).

Keywords: Quantum Materials • EuB_6 • YbB_6 • LaB_6 •Vibronic Effects • Chemical Bonding

[1] L. Jiao, S. Rößler, D, J. Kim, L. H. Tjeng, Z. Fisk, F. Steglich, S. Wirthiao, *Nat. Commun.* **2016**, *7*, 13762.
[2] M. C. Aronson, R. Osborn, R. A. Robinson, J. W. Lynn, R. Chau, C. L. Seaman, M. B. Maple, *Phys. Rev. Lett.* **1995**, *75*, 725-728.
[3] D. Chowdhury, I. Sodemann, T. Senthil, Nat. Commun. 2018, 9, 1766.
[4] C. Zeng, Y. Chen, K. Iida, K. Nobusada, K. Kirschbaum, K. J. Lam-bright, R. Jin, R, *J. Am. Chem. Soc.* **2016**, *138*, 3950-3953.
[5] M. Dzero, J. Xia, V. Galitski, P. Coleman, *Annu. Rev. Condens. Matter Phys.* **2016**, *7*, 249-280.
[6] B. B. Zhou, M. Misra, E. H. da Silva Neto, P. Aynajian, R. E. Baumbach, J. D. Thompson, E. D. Bauer, A. Yazdani, *Nat. Phys.* **2013**, *9*, 474-479.
[7] H. M. Weng, J. Z. Zhao, Z. J. Wang, Z. Fang, X. Dai, *Phys. Rev. Lett.* **2014**, *112*, 016403.
[8] L. M. Falicov, J. C. Kimball, *Phys. Rev. Lett.* **1969**, *22*, 997-999.
[9] G. Li, Z. Xiang, F. Yu, T. Asaba, B. Lawson, P. Cai, C. Tinsman, A. Berkley, S. Wolgast, Y. S. Eo, D. J. Kim, C. Kurdak, J. W. Allen, K. Sun, X. H. Chen, Y. Y. Wang, Z. Fisk, L. Li, *Science* **2014**, *346*, 1208-1212.
[10] M. Pohlit, S. Rößler, Y. Ohno, H. Ohno, S. von Molnár, Z. Fisk, J. Müller, S. Wirth, *Phys. Rev. Lett.* **2018**, *120*, 257201.
[11] H. Jang, G. Friemel, J. Ollivier, A. V. Dukhnenko, N. Y. Shitsevalova, V. B. Filipov, B. Keimer, D. S. Inosov, *Nat. Mater.* **2014**, *13*, 682-687.
[12] W. –L. Li, C. Ertural, D. Bogdanovski, J. Li, R. Dronskowski, *Inorg. Chem.* **2018**, *57*, 12999-13008.
[13] W. A. Phelan, S. M. Koohpayeh, P. Cottingham, J. W. Freeland, J. C. Leiner, C. L. Broholm, T. M. McQueen, *Phys. Rev. X* **2014**, *4*, 031012.
[14] L. Degiorgi, E. Felder, H. R. Ott, J. L. Sarrao, Z. Fisk, *Phys. Rev. Lett.* **1997**, *79*, 5135-5137.
[15] L. Sun, Q. Wu, *Rep. Prog. Phys.* **2016**, *79*, 084503.
[16] N. P. Butch, J. Paglione, P. Chow, Y. Xiao, C. A. Marianetti, C. H. Booth, J. R. Jeffries, *Phys. Rev. Lett.* **2016**, *116*, 156401.
[17] M. K. Blomberg, M. J. Merisalo, M. M. Korsukova, V. N. Gurin, *J. Alloys Compd.* **1995**, *217*, 123–127.
[18] T. Nanba, M. Tomikawa, Y. Mori, N. Shino, S. Imada, S. Suga, S. Kimura, S. Kunni, *Physica B Condens. Matter* **1993**, *186-188*, 557-559.
[19] L. Bai, N. Ma, *Physica B* **2010**, *405*, 4634-4637.
[20] M. Amara, S. E. Luca, R. –M. Galéra, *Phys. Rev. B* **2005**, *72*, 064447.
[21] M. E. Zhitomirsky, T. M. Rice, V. I. Anisimov, *Nature* **1999**, *402*, 251.
[22] P. J. Robinson, X. Zhang, T. McQueen, K. H. Bowen, A. N. Alexandrova, *J. Phys. Chem. A* **2017**, *121*, 1849-1854.
[23] J. Munárriz, R. Laplaza, A. M. Pendás, J. Contreras-García, *Phys. Chem. Chem. Phys.* **2019**, *21*, 4215-4223.
[24] A. N. Alexandrova, *Chem. Mater.* **2017**, *29*, 8555-8565.
[25] P. J. Robinson, J. Munarriz, M. E. Valentine, A. Granmoe, N. Drichko, J. R. Chamorro, P. F. Rosa, T. M. McQueen, A. N. Alexandrova, *Angew. Chem. Int. Ed.* **2020**, DOI: https://doi.org/10.1002/ange.202000945.
[26] J. Munárriz, R. Laplaza, V. Polo, *Mol. Phys.* **2019**, *117*, 1315-1324.
[27] P. J. Robinson, G. Liu, S. Ciborowski, C. Martinez-Martinez, J. R. Chamorro, T. M. McQueen, K. H. Bowen, A. N. Alexandrova, *Chem. Mater.* **2017**, *29*, 9892-9896.
[28] W. –L. Li, T. –T. Chen, D. –H. Xing. X. Chen, J. Li, L. –S. Wang, *Proc. Natl. Acad. Sci. U.S.A.* **2018**, *115*, E6972–E6977.
[29] H. Martinho, C. Rettori, G. M. Dalpian, J. L. F. da Silva, Z. Fisk, S. B. Oseroff, *J. Phys.: Condens. Matter* **2009**, *21*, 456007.
[30] M. A. Anisimov, V. V. Glushkov, A. V. Bogach, S. V. Demishev, N. A: Samarin, A. Yu. Gavrilkin, K. V. Mitsen. N. Yu. Shitsevalova, A. V. Levchenko, V. B. Filippov, S. Gabani, K. Flachbart, N. E. Sluchanko, J. Exp. Theor. Phys. 2013, 16, 760-765.
[31] X. Zhang, L. Yu, S. von Molnár, Z. Fisk, P. Xiong, *Phys. Rev. Lett.* **2009**, *103*, 106602.
[32] U. Yu, B. I. Min, *Phys. Rev. B* **2006**, *74*, 094413.
[33] K. Takegahara, M. Kasaya, T. Goto, T. Kasuya, *Physica* **1985**, *130B*, 49-51.
[34] H. G. Smith, G. Dolling, S. Kunii, M. Kasaya, B. Liu, K. Takegahara, T. Kasuya, T. Goto, *Solid State. Commun.* **1985**, *53*, 15-19.
[35] J.Ying, L. Tang, F. Chen, X. Chen, V. V. Struzhkin. *Phys. Rev. B* **2018**, *97*, 121101.
[36] N. Ogita, S. Nagai, N. Okamoto, M. Udagawa, F. Iga, M. Sera, J. Akimitsu, S. Kunii, *Phys. Rev. B* **2003**, *68*, 224305.
[37] D. Mandrus, B. C. Sales, R. Jin, *Phys. Rev. B* **2001**, *64*, 012302.
[38] J. T. Cahill, O. A. Graeve, *J. Mater. Res. Technol.* **2019**, 8, 6321-6335.
[39] Otani, S., Honma, S., Tanaka, T., Ishizawa, Y. *J. Alloys Compd.* **1992**, 179, 201-205.
[40] Bogach, A. V., Glushkov, V. V., Demishev, S. V., Sluchanko, N. E., Shitsevalova, N. Y., Fillipov, V. B., Flachbart, K. *Solid State Sci.*, **2012**, 14, 1629-1631.
[41] Tarascon, J. M., Isikawa, Y., Chevalier, B., Etoumeau, J., Hagenmuller, P., Kasaya, M. *J. Phys.* **1980**, 41(10), 1135-1140.
[42] Aivazov, M. I., Bashilov, V. A., Zinchenko, K. A., Kagramanova, R. R. *Soviet Powder Metallurgy and Metal Ceramics*, **1979**, 18, 37-39.
[43] Mercurio, J. P., J. Etourneau, R. Naslain, and P. Hagenmuller, *J Less Common Met* **1976** 47, 175-180.
[44] Rhyee, J. S., Cho, B. K. *J. Appl. Phys*, 97, 10A901.
[45] Snow, C. S., Cooper, S. L., Young, D. P., Fisk, Z., Comment, A., Ansermet, J. P. *Phys. Rev. B* **2001** 64, 174412.
[46] Rhyee, J. S., Kim, J. Y., Cho, B. K., Lee, H. J., Kim, H. C., Park, H. M. Phys. Rev. B **2006** 74, 235114.
[47] Song, M., Yang, I. S., Seo, C. W., Cheong, H., Kim, J. Y., Cho, B. K. *J. Magn. Magn. Mater.* ***2007*** 310, 1019-1020.
[48] Z. Xiag, S. Y. Rodriguez, L. Saribaev, J. H. Ross Jr., *Phys. Rev. B.* **2012** 85, 214304.
[49] Dahm, Thomas, and Kazuo Ueda, *Phys. Rev. Lett.* **2007**, 99, 187003.
[50] Caldwell, T., A. P. Reyes, W. G. Moulton, P. L. Kuhns, M. J. R. Hoch, P. Schlottmann, and Z. Fisk, *Phys. Rev. B* **2007,** 75, 075106.
[51] Mo, S-K., G-H. Gweon, J. D. Denlinger, H-D. Kim, J. W. Allen, C. G. Olson, H. Höchst, J. L. Sarrao, and Z. Fisk, *Physica B* **2002** 312, 668-669.